Materials Today Bio 18 (2023) 100533

Contents lists available at ScienceDirect

Materials Today Bio

journal homepage: www.journals.elsevier.com/materials-today-bio

In-vivo bone remodeling potential of Sr-d-Ca-P /PLLA-HAp coated biodegradable ZK60 alloy bone plate

Seong-Su Park [a], Ume Farwa [b], Ihho Park [c], Byoung-Gi Moon [c], Soo-Bin Im [b,d], Byong-Taek Lee [a,b,*]

[a] Department of Regenerative Medicine, College of Medicine, Soonchunhyang University, Cheonan, South Korea
[b] Institute of Tissue Regeneration, Soonchunhyang University, Cheonan, South Korea
[c] Korea Institute of Material Science, Changwon, South Korea
[d] Department of Neuro-surgery, Soonchunhyang University Medical Centre, Bucheon, South Korea

ARTICLE INFO

Keywords:
Magnesium alloy
Bone plate
Sr-D-Ca-P/PLLA-HAp coating
Bone remodeling
Corrosion resistance

ABSTRACT

Magnesium and its alloys are widely applied biomaterials due to their biodegradability and biocompatibility. However, rapid degradation and hydrogen gas evolution hinder its applicability on a commercial scale. In this study, we developed an Mg alloy bone plate for bone remodeling and support after a fracture. We further coated the Mg alloy plate with Sr-D-Ca-P (Sr dopped Ca–P coating) and Sr-D-Ca-P/PLLA-HAp to evaluate and compare their biodegradability and biocompatibility in both *in vitro* and *in vivo* experiments. Chemical immersion and dip coating were employed for the formation of Sr-D-Ca-P and PLLA-HAp layers, respectively. *In vitro* evaluation depicted that both coatings delayed the degradation process and exhibited excellent biocompatibility. MC3T3-E1cells proliferation and osteogenic markers expression were also promoted. *In vivo* results showed that both Sr-D-Ca-P and Sr-D-Ca-P/PLLA-HAp coated bone plates had slower degradation rate as compared to Mg alloy. Remarkable bone remodeling was observed around the Sr-D-Ca-P/PLLA-HAp coated bone plate than bare Mg alloy and Sr-D-Ca-P coated bone plate. These results suggest that Sr-D-Ca-P/PLLA-HAp coated Mg alloy bone plate with lower degradation and enhanced biocompatibility can be applied as an orthopedic implant.

1. Introduction

Bone plates are widely used for fractured bone repair where the bone plate is fixed to the fracture site with screws. For a bone plate to be effective, it must withstand all the mechanical forces acting on the fracture [1]. The incredible mechanical properties and biodegradability of magnesium-based alloys have allured many scientists [2–6]. The biodegradability of Mg-based alloys after implantation eliminates the need for secondary surgery [3,7]. The resemblance of physical properties of the Mg-based alloys like elastic modulus and density with those of human bones renders them valuable implants for bone regeneration [8]. However, their fast degradation in physiological environments impedes their commercial application [9]. To overcome this problem, the surface coating has been shown to be an efficient and simple technique [10]; the coating process controls the degradation of the Mg alloys and improves biocompatibility. The outcomes of an optimal biomaterial coating should be biocompatibility, nontoxicity, and a slower degradation rate corresponding to the healing time [11,12]. A variety of the coatings such as, organic, inorganic, and inorganic-organic coatings have been explored to decrease the fast degradation of the Mg. For the bone-based bio-implant, bioactive calcium phosphate coating (Ca–P) is a favorable choice as the Ca and P are the main components of the bone [13]. This type of coating improves the biodegradability and biocompatibility of the Mg implants. Amongst various paths adopted for the coating process, chemical immersion and dip coating are the most economical and simple techniques for implants with complex shapes.

Strontium (Sr), found as a trace element, has the natural ability to support the osteoblast differentiation, while simultaneously delaying osteoclast proliferation and growth [14,15]. Sr also controls bone remodeling by retarding bone resorption and enhancing the bone formation process [16,17]. Sr based coating on the Mg alloys has been explored widely for increased bioactivity and corrosion resistance of implants [18]. The exploration of Sr dopped Ca–P coating has been mostly limited to *in vitro* studies [19–25]. However, a few studies have reported the effects of Sr dopped Ca–P coating *in vivo* [26]. The *in vivo* results showed a promising decrease in degradation of Sr dopped Ca–P

* Corresponding author. Department of regenerative medicine, College of Medicine, Soonchunhyang University, Cheonan, South Korea.
E-mail address: lbt@sch.ac.kr (B.-T. Lee).

https://doi.org/10.1016/j.mtbio.2022.100533
Received 26 October 2022; Received in revised form 12 December 2022; Accepted 26 December 2022
Available online 27 December 2022

coated implant as compared to bare Mg alloy as reported by our group previously [27]. However, the brittle nature of the Sr dopped Ca–P coating (Sr-D-Ca-P) results in uneven coating consequently creating gaps between the metal surface and the coated materials. These gaps can provide pathways for the external ion-rich fluids to penetrate the metal surface and fasten the degradation process. There is a need to fill these gaps to provide a compact resistance against corrosion.

Hydroxyapatite (HAp) has excellent bone regenerative properties owing to its higher bioactivity, biocompatibility, osteoconductive non-toxicity, non-inflammatory behavior, and slower degradation [28–30]. However, despite the excellent bioactivity, its coating is brittle and therefore susceptible to plastic deformation under mechanical stress. Consequently, there are high chances of crack formation in the protection layer during implant surgery or after the implantation due to considerable levels of mechanical stress [31,32].

Amongst the various types of coating materials available, biodegradable polymers such as poly (*l*-lactide) acid (PLLA), poly (ε-caprolactone) (PCL), and poly (lactide-*co*-glycolide) (PLGA) are flexible and can withstand higher levels of mechanical stress [32,33]. However, due to weak bonding between the Mg surface and the polymers coating, there are chances of interfacial delamination and subsequent effects on the Mg alloy biodegradability [34]. Bare polymer coating in the case of orthopedic application decreases the bioactivity as formation of apatite is not favored. To favor the apatite formation, addition of HAp in polymer coating such as PLLA is an innovative approach. The polymer coating can decrease the degradation rate whereas incorporated HAp particles can increase the bioactivity for orthopedic application.

Notably, combined organic and inorganic coating has been less explored. A ceramic coating containing calcium, phosphorous, and other inorganic ions can help to elevate the biocompatibility of the coating material. It can also enhance bone remodeling which consequently strengthens the fractured site. Polymeric coating can shield the fast degradation of the brittle inorganic coating or ceramic coating, therefore, enhancing the bone plates' characteristics.

In this study, we report the dual Inorganic/Polymeric-ceramic (Sr-D-Ca-P/PLLA-HAp) coating on Mg alloy (ZK60) implant as a supporting plate for the fractured bone. Our previous results indicated that Sr-D-Ca-P coating on Mg alloy can successfully lower the degradation rate of Mg alloy [27]. We hypothesized that Sr-D-Ca-P inner coating will support better adherence to the PLLA coating, accompanied by HAp particles for improved bioactivity. Sr-D-Ca-P is not a compact coating with vacant spaces at the interface of Mg alloy and the coating, which results in fast degradation. By adding PLLA-HAp the vacant spaces can be filled and the degradation rate can be decreased dramatically. The substrate Mg alloy ZK60 is used due to its biodegradable, nontoxic alloying elements (zinc and zirconium), and mechanical properties comparable to the cortical bone [35,36]. The combined effects of the two coatings will lower the degradation rate and increase the bioactivity of the implant. The bioactivity of the bone plate will induce bone remodeling and the formation of the new bone surrounding the implanted bone plate will strengthen the fracture site as the bone plate slowly degrades. To evaluate our hypothesis, we first performed *in vitro* compatibility test. Further, *in vivo* experiments were conducted in a rabbit model for one and two months to evaluate biodegradation and biocompatibility.

2. Material and methods

2.1. Sample preparation

For the *in vitro* evaluation, Mg alloy ZK60 (Zn-5.5%, Zr-0.49%, and Mg balance) was cut to a size of 10 mm × 10 mm x 2 mm. For *in vivo* experiments, a bone plate of 20 mm × 8 mm x 2 mm was prepared. Then, samples were mechanically polished with silicon carbide (SiC) paper from 800 to 1500 grit size followed by a diamond paste. To obtain the grain boundaries, etching was performed utilizing etching solution (ethanol 70 mL, distilled water 10 mL, picric acid 4.2 g, and acetic acid 10 mL) for 10 s [37]. All the chemicals used in this process were obtained from Samchun Pure Chemical Ltd., Korea. An optical microscope (BX51RF, Olympus, Japan) was utilized to observe the etched surface.

To obtain the Sr-D-Ca-P coating, the samples were polished with SiC paper (800–1500 grit size), washed with acetone and water ultrasonically, and followed by drying at room temperature. Then, the samples were immersed in an electrolytic bath for 24 h at 70 °C [20] which was prepared by dissolving 36 g of calcium nitrate tetrahydrate ($Ca(NO_3)_2{\cdot}4H_2O$), 16 g of sodium dihydrogen phosphate dihydrate ($NaH_2PO_4{\cdot}2H_2O$), and 4 g of strontium nitrate ($Sr(NO_3)_2$) separately in 1 L distilled water. After the process of deposition, the samples were washed with distilled water before further use.

For the PLLA-HAp coating, PLLA (Poly (L-lactide, Sigma-Aldrich, mol. Wt. 85,000–160,000) (2%) was dissolved in dichloromethane (DCM) to obtain a clear solution. In the PLLA solution, HAp (particle size:10–40 nm) [38] 20% was added and further stirred to obtain a slurry. Air-dried Sr-D-Ca-P coated samples were dipped in the solution and retrieved at a speed of 1 mm/s. Samples were then dried in a vacuum. All the reagents used in the coating process were obtained from Sigma Aldrich, USA.

2.2. Coating characterization

To observe the surface morphologies of the Mg, Sr-D-Ca-P, and Sr-D-Ca-P/PLLA-Hap, scanning electron microscopy (SEM, JSM-635 F, JEOL, Tokyo, Japan) supplied with an energy dispersive X-ray spectrometer (EDX, Oxford Instruments, UK) was used. Before conducting SEM, sputter coating of platinum (Pt) was developed on samples (Cressington 108 Auto, JEOL, Tokyo, Japan). The surface roughness of the coating was determined by the AFM (Atomic force microscopy, XE-150, PSIA). TEM (transmission electron microscopy, 200 kV, F-20 (FEI)) was employed to evaluate the cross-sectional morphology of the Ca–Sr–P and Ca–Sr–P/PLLA-HAp coating. Protected Pt (platinum ~1 μm) was deposited which was later trenched. TEM slicing was conducted by applying 0.24 nA and 18 pA current for bulk milling and final thinning, respectively. To determine the phases in the samples, X-ray diffraction (XRD, D/MAX-250, Rigaku, Japan) with Cu Kα radiation was carried out. To determine the diffraction patterns, 2θ was used with values ranging from 10° to 80°. The scanning speed was set as 1°/min. To determine the wetting angle of the samples, DSA 100, KRUSS GmbH instrument was utilized. For this purpose, distilled water was used, with a 1 μls^{-1} dosage rate and 10 μl volume drops. For each measurement, six readings were considered. Surface analysis was also performed with XPS (Thermo Scientific K-Alpha X-ray Photoelectron Spectrometer). The source of the radiation was AlKα with scanning range of 0–1350 eV. Scratch test was conducted to evaluate the critical load of the surface using (Anton Paar Micro Combo Tester, Austria). The load was increased progressively from 10 mN to 20,000 mN. The scratch scanning area was 1000 μm. Rockwell diamond ball having a radius of 100 μm tip was used with the velocity of the indenter was 10 μm/s.

2.3. In vitro degradation

To determine the *in vitro* degradation of the Mg alloy, Sr-D-Ca-P and Sr-D-Ca-P/PLLA-HAp coated samples, an immersion test was conducted following the standard protocols (ASTM G31-72). Before immersion of the samples in the hank solution (Gibco, Korea, pH-7.4), the initial weight (W_0) of the samples was recorded. The immersion test was performed for 14 days at 37 °C. For the immersion test, 50 mL/cm^2 of the volume to area ratio was used. The solution was replaced daily with a fresh solution, along with the determination of the pH (Thermo Scientific, Korea). To determine the weight loss each sample was removed from the solution at predestined time points (i.e., 3, 7, 10, and 14 days), cleaned with chromic acid followed by washing with distil water, dried, and then weighed (W_1). The following equation was used to determine the weight loss.

$$W_S = [\,(W_1 - W_0)\ /\ W_0]^* 100$$

Here, Ws refers to percentage weight loss, initial weight is denoted by W_0, and the final weight is referred to as W_1. An immersion test was performed in triplicate for each sample. To observe the release of hydrogen gas, samples were immersed in Hank's solution and an inverted graduated test tube was placed. This system was placed at 37 °C and release was monitored for 14 days. For the hydrogen gas release and pH change, each set was repeated in triplicate. The samples were immersed in 10 mL of SBF (stimulated body fluid) to determine the *in vitro* bioactivity. The samples were incubated at 37 °C for 14 days. Each day the SBF solution was replaced with a fresh one. SBF was prepared following a previously developed method [39]. After 14 days, the immersed samples were taken out, washed with distilled water followed then dried. SEM and EDS analyses were performed to determine the surface morphology and chemical composition, respectively.

2.4. In vitro biocompatibility

To evaluate the cell viability and cell proliferation, pre-osteoblast MC3T3-E1 cells (ATCC, CRL-2593, the American Type Culture Collection, USA) were utilized. The media used to culture the cells contained, minimum essential medium, α-MEM (Gibco, USA) supplemented with 10% fetal bovine serum FBS (Sigma Aldrich, USA), 1% penicillin-streptomycin, and PS (Bio-Whittaker, USA). To maintain the cells a humidified incubator at 37 °C with 5% CO_2 was used.

Cell viability was evaluated by the direct MTT assay. Sr-D-Ca-P and Sr-D-Ca-P/PLLA-HAp coated samples were placed in a 12-well plate and sterilized by UV for 40 min. Then each sample was seeded with 1×10^4 cells/mL. Cells seeded in the 12 well plates without samples were considered as the positive controls. The cell-seeded samples were maintained for 1, 3, and 7 days at 37 °C with 5% CO_2. To carry out the MTT assay protocol, samples loaded with cells were removed from the incubator at 1, 3, and 7 days, and 200 μl of MTT [3-(4,5-dimethylthiazol-2-yl)-2,5 diphenyltetrazolium bromide] solution (Gibco, CA) was added to each well and maintained for 4 h at 37 °C. After that, 200 μl of dimethyl sulfoxide (DMSO) (Samchun Chemical, South Korea) was added and incubated for 1 h. To determine the optical densities, an ELISA reader (EL 312, Biokinetics reader, Bio-Tek instrument) was used at a wavelength of 595 nm.

Cell proliferation profile was developed by seeding 1×10^4 cells/mL MC3T3-E1 cells on the sterilized samples, in a 24-well plate. Cell seeded wells without the sample were considered as the control. The cell-seeded wells were incubated for 1, 3, and 7 days in a humidified incubator at 37 °C with 5% CO_2. After incubation, at a predetermined time, washing was performed with PBS (Sigma Aldrich, USA) three times. After washing, the fixation process was done with 4% paraformaldehyde (Sigma Aldrich, USA) for 10 min. 0.5% Triton X-100 (Sigma Aldrich, USA) was used for permeabilization for 10 min, followed by blocking with 2.5% bovine serum albumin, (BSA Sigma-Aldrich, USA) for 1 h. Blocking was done at room temperature. After the blocking process, the samples were immunostained with fluorescein isothiocyanate (FITC) conjugated phalloidin solution (Sigma Aldrich, USA) 25 μg/mL at 4 °C for 12 h. Nuclei were stained with Hoechst (Sigma Aldrich, USA) at 10 μg/mL for 5 min. To observe the cell proliferation confocal microscope (Olympus, FV10i-W, USA) accompanied by FV10i-ASW2.0 software was used.

2.5. In vitro osteogenic property

To determine the osteogenic properties of the Mg alloy, Sr-D-Ca-P and Sr-D-Ca-P/PLLA-HAp coated samples, MC3T3-E1 cells were seeded on the surface of the samples. Osteogenic media used for this purpose consisted of 1% penicillin-streptomycin, α-MEM supplemented with 10% FBS, 10 nM dexamethasone (Sigma Aldrich, USA), 50 μg/mL L-ascorbic acid (Sigma Aldrich, USA), and 10 mM β-glycerophosphate disodium salt hydrate (Sigma Aldrich, USA). To carry out real-time PCR (q-PCR) analysis, total RNA was extracted from the cells following the manufacturer's protocol of ReboEX (Geneall, South Korea) and Hybrid R (Geneall, South Korea). A nanodrop (Thermo Fisher Scientific, USA) was used to determine the total concentration of the RNA. Using the Maxime RT PreMix kit (LiliF, Korea), 2 μg of RNA was converted to cDNA. q-PCR on the StepOne™ RealTime PCR System (Thermo Fisher, USA) with PowerUp™ SYBR™ Green Master Mix (Applied Biosystems, USA) was used to determine the gene expression of the samples. Osteoblastic markers OPN (Osteopontin), OCN (Osteocalcin), ALP (Alkaline phosphatase), and GAPDH (Glyceraldehyde-3-phosphate dehydrogenase) levels of mRNA were determined. The control used here is GAPDH. The sequence of the primers is listed in Table 1.

Table 1
Primer sequences for real-time PCR analysis.

Primer	Sequence
mGapdh F	tctcctgcgacttcaaca
mGapdh R	ctgtagccgtattcattgtc
mOPN F	gatgatgatgacgatggagac
mOPN R	gactgtagggacgattgga
mALP F	ccaactcttttgtgccagaga
mALP R	ggctacattggtggtgagacttttt
mOCN F	gcttaaccctgcttgtga
mOCN R	tcctaaatagtgataccgta

F= Forward, R = Reverse.

2.6. In vivo implantation

To evaluate the degradation behavior of the dual-coated bone plates, *in vivo* experiment was conducted. For this purpose, eighteen New Zealand white rabbits (12 weeks, ~2.5 kg) were used. Three samples consisting of Mg alloy, Sr-D-Ca-P, and Sr-D-Ca-P/PLLA-HAp coated bone plates were analyzed. Animal experiments were carried out after approval from the Soonchunhyang University Institutional Animal Care and Use Committee and cared according to the provided guidelines (Approval no: SCH 21-0031). Rabbits used in these experiments were acquired from DBL (South Korea). To anesthetize the animals, an isoflurane vaporizer (Piramal Critical Care Inc., USA) in combination with oxygen was used. The right leg of the rabbit was shaved to uncover the femur bone, and the area was sterilized with 70% ethanol and povidone-iodine solution. An incision was made, and overlying skin and muscle were carefully retracted to expose the shaft. To prevent tissue dehydration, continuous irrigation with saline solution was provided. Mg alloy, Sr-D-Ca-P, and Sr-D-Ca-P/PLLA-HAp coated bone plates were placed on the shaft and fixed with a screw. Then, the surgery site was closed and sutured. To prevent infection and minimize the pain, an antibiotic, Baytril (Bayer Co., Korea), and a painkiller, Maritrol (Jeil pharmaceutical, Korea) were administered for three days. After one and two months animals were sacrificed by CO_2 inhalation.

2.7. Micro CT analysis

The desired tissue sections were fixed using 10% buffered formalin. A micro-CT scanner (SkyScan 1172, Bruker, Belgium) was used to scan the fixed samples and evaluate the degradation rate of metal plates. NRecon software was used to reconstruct the scanned data. To investigate the degradation rate of the metal plates, reconstructed images were imported to CTAn (SkyScan) and CTVol (SkyScan) software.

2.8. Histological analysis

Formalin-fixed samples were washed with running tap water for 4 h to remove any residual acid. Dehydration of the samples was performed using a standard series of ethanol (70–100%). After dehydration samples were dipped in acetone to eliminate any residual ethanol. For embedding methyl methacrylate (MMA) (Sigma Aldrich, South Korea) resin along

with benzoyl peroxide (Sigma Aldrich, South Korea) were used. A diamond abrasive cutter (R&B, South Korea) was used to cut the samples while polishing up to a 10–45 μm thickness. Multiple stain solution (MSS) was applied to stain the tissue slides. An optical microscope (BX53 Olympus, USA) provided with a DP72 digital camera was used to analyze and capture images.

2.9. Statistical analysis

GraphPad Prism version 8.0 (GraphPad Software, Inc., USA) was used to perform all the statistical analyses. Two variance analysis ANOVA and *t*-test were utilized to compare different groups. $P < 0.05$ was considered as confidence level unless otherwise stated. The experiments are performed in triplicate ($n = 3$), unless mentioned otherwise.

3. Results and discussion

3.1. Coating characterization

The optical microstructure of ZK60 after the etching process presented course and equiaxed grains of approximately 100–200 μm (Fig. 1a). Magnesium-zinc (MgZn) intermetallic phase was observed in the form of precipitates at the grain boundaries and inside the grains [40].

SEM images of the Sr-D-Ca-P and Sr-D-Ca-P/PLLA-HAp are depicted in Fig. 1b and c. The surface morphology of the Sr-D-Ca-P coated Mg plate showed crystalline Sr dopped Ca–P structures. The densely covered surface was defect-free and uniform. Sr-D-Ca-P/PLLA-HAp showed a surface covered with PLLA entrapped HAp particles. HAp particles are seen in aggregated form in the coating. The composition of the coating was confirmed by the EDS analysis. The EDS analysis of the Sr-D-Ca-P coated sample displayed phosphorous (P), strontium (Sr), oxygen (O), and calcium (Ca) elements. The presence of Sr peak along with Ca and P is an indication of the successful doping of Sr in calcium and phosphorous coating. Sr-D-Ca-P/PLLA-HAp coated samples showed the presence of carbon (C), oxygen (O), phosphorous (P), and calcium (Ca) elements. The 3D AFM images of the three coated surfaces are displayed in (Fig. 1d–f). The surface of Mg alloy is polished before coating, so from the AFM images visible surface waviness is observed. The surface morphologies of the coated surfaces Sr-D-Ca-P and Sr-D-Ca-P/PLLA-Hap are observed in AFM similar to the SEM images.

To analyze the coating interfaces, samples were cross-sectionally cut and observed by SEM (Fig. 1g–h), TEM (Fig. S2). In the Sr-D-Ca-P coated sample the intersection between the Mg alloy and Sr-D-Ca-P was distinguishable (Fig. 1g). Columnar structures were observed with vacant spaces between the coating and Mg alloy surface (Fig. S2). This can cause serious delamination and debonding of the coating, consequently increasing the degradation rate by fluid penetration to the surface and

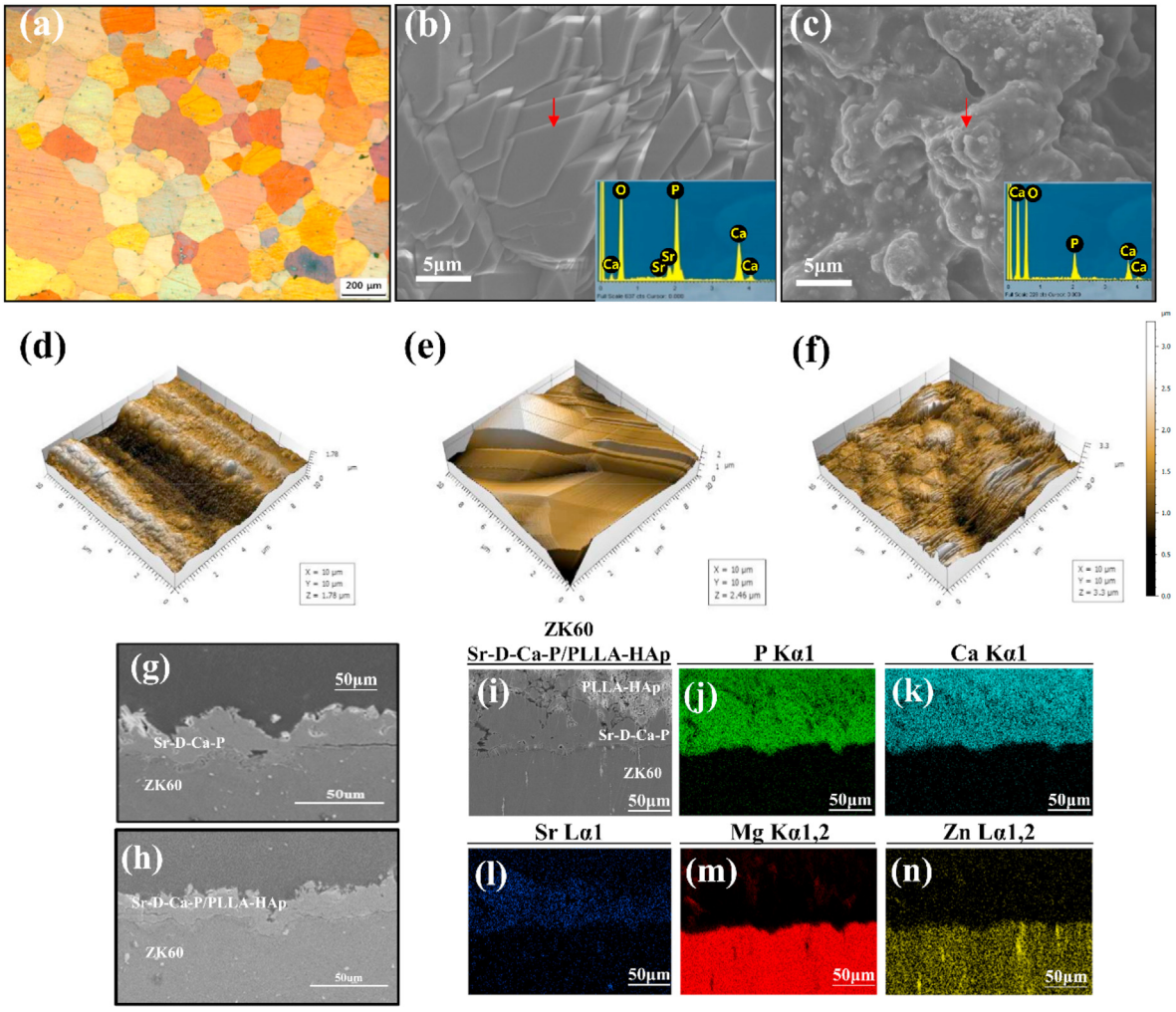

Fig. 1. Surface morphology of bare ZK60, Sr-D-Ca-P coated, and Sr-D-Ca-P/PLLA-HAp coated bone plate; (a) Optical micrograph of ZK60, SEM images and EDS profiles of (b) Sr-D-Ca-P coated bone plate (c) PLLA-HAp coated bone plate, AFM images of (d) ZK60 (e) Sr-D-Ca-P and (f) Sr-D-Ca-P/PLLA-HAp. Cross sectioned interface of (g) ZK60/Sr-D-Ca-P and (h,i) ZK60/Sr-D-Ca-P/PLLA-HAp observed by SEM, and (j–n) EDS mapping profile of ZK60/Sr-D-Ca-P/PLLA-HAp coating.

hydrogen gas evolution. The hydrogen gas bubble can delaminate the coating. On the opposite side, Sr-D-Ca-P/PLLA-HAp coated bone plate did not show such delamination behavior. The polymer coating filled the vacant spaces created by Sr-D-Ca-P deposition. The strong adherence between the PLLA and the inorganic Sr-D-Ca-P coating prevents delamination. Previously polymer coatings have been proved to decrease the degradation process significantly [41]. Nevertheless, in the case of orthopedic applications, the bare polymer coating can somehow decrease the bioactivity as apatite formation is not favored in alone polymer coated surfaces [42]. The incorporation of HAp particles in PLLA is an excellent approach to decrease the degradation process without compromising bioactivity.

The EDS mapping profile of the Sr-D-Ca-P/PLLA-HAp bone plate showed the deposition of magnesium, zinc, calcium, strontium, and phosphate. Calcium (Ca), strontium (Sr), and phosphate (P) represented by cyan, blue, and green colors, respectively were observed on the outer layer of the bone plate (Fig. 1i-n). Zinc (Zn) and magnesium (Mg) denoted by yellow and red color, respectively, were observed as the base material located in the inner layer (Fig. 1m,n). Sr-D-Ca-P coating layer shows Ca, Sr and P, whereas PLLA-HAp layer show Ca and P elements.

The XRD analysis for Mg alloy, Sr-D-Ca-P, and Sr-D-Ca-P/PLLA-HAp coating is displayed in Fig. 2a. The characteristic peaks of Mg for the hexagonal structure were detected in the Mg alloy XRD spectrum (ICDD No: 01-071-6543). In the Sr-D-Ca-P coated samples calcium strontium phosphate ($Ca_2Sr(PO_4)_2$, ICDD No: 00-052-0467) and dicalcium phosphate ($CaHPO_4{\cdot}2H_2O$, ICDD No: 01-075-4372) peaks were identified along with Mg peaks. In the case of Sr-D-Ca-P/PLLA-HAp, the identifying peaks for HAp were observed (ICDD NO: 01-074-0566). The Sr-D-Ca-P peaks are weak as there are two types of components present, both amorphous and crystalline as proved by the electron diffraction pattern (Fig. S4). In the dual Sr-D-Ca-P/PLLA-HAp coating the Sr-D-Ca-P peaks are very weak, this can be assorted to the polymer coating covering the Sr-D-Ca-P surface.

Evaluation of the surface hydrophilicity is an important parameter to evaluate cell proliferation and cell attachment. The surfaces with higher hydrophilicity promote cell proliferation and cell attachments [43,44]. The wettability measurements of the Mg alloy, Sr-D-Ca-P, and Sr-D-Ca-P/PLLA-HAp coated surface is depicted in Fig. 2b. The results indicate that as compared to Mg alloy and Sr-D-Ca-P coated surface, Sr-D-Ca-P/PLLA-HAp dual coated surface showed enhanced hydrophilicity. The wetting angle of the Mg alloy, Sr-D-Ca-P, and Sr-D-Ca-P/PLLA-HAp were 113.1°, 109.6°, and 70.4°, respectively. The hydrophobic nature of the Sr-D-Ca-P can be assorted to the low surface energy of the coating [45].

Surface chemical state of the electrons was determined by the XPS analysis (Fig. 2c). The XPS analysis of the Mg surface showed peaks for Mg, C, and O. The humidity in the air can result in the formation of $Mg(OH)_2$ or some hydrocarbons which might be the source of oxygen peak appeared in the XPS spectra of the Mg [46]. The carbon peak is also assorted to the environmental contaminations. The Sr-D-Ca-P coating showed the corresponding peaks for Sr, O, C, Ca, and P. The appearance of the two characteristic peaks Sr peaks for Sr2p and Sr3d confirmed the doping of Sr at the surface [27]. The Sr-D-Ca-P/PLLA-HAp dual coated surface indicated the presence of Ca, P, C, and O. Carbon and oxygen can be assorted to the corresponding to the PLLA and calcium and phosphorous indicating the HAp peaks. The adhesion test results for Sr-D-Ca-P and Sr-D-Ca-P/PLLA-HAp showed a value of 7.6 N and 13.9 N, respectively (Fig. 2d). The results demonstrate that Sr-D-Ca-P/PLLA-HAp adhere more strongly as compared to the single Sr-D-Ca-P layer. Sr-D-Ca-P coating is not even, with cracks. The TEM image (Fig. S2) of the interface between the Sr-D-Ca-P coating and Mg metal shows that columnar structures are formed which are uneven with a lot of empty spaces in between. When PLLA-HAp coating is applied on the Sr-D-Ca-P coating, the cracks and gaps are filled completely. This results in a strongly adhering dual coating with less delamination as compared to the single Sr-D-Ca-P coating.

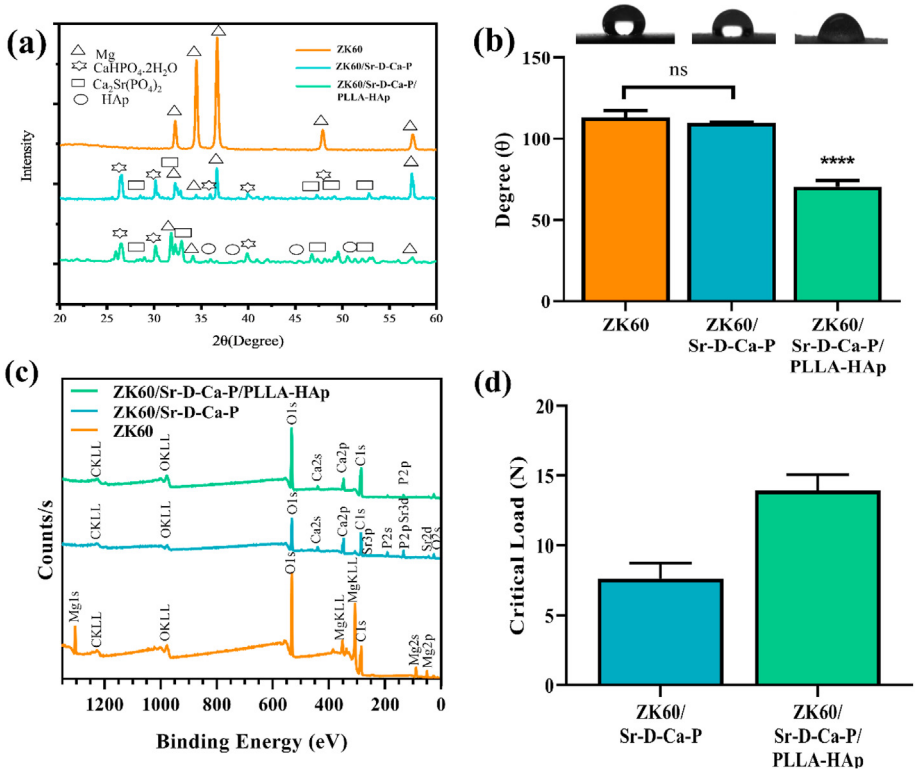

Fig. 2. (a) XRD, (b) wetting angle, (c) XPS analysis of ZK60, ZK60/Sr-D-Ca-P, and ZK60/Sr-D-Ca-P/PLLA-HAp coated samples, and (d) adhesion strength of Sr-D-Ca-P, and ZK60/Sr-D-Ca-P/PLLA-HAp coated samples (n.s: not significant) (****$p < 0.0001$).

3.2. Biodegradation

The immersion test was performed to investigate the *in vitro* degradation profile of the samples. All the samples (Mg alloy, Sr-D-Ca-P and Sr-D-Ca-P/PLLA-HAp) were immersed in Hank's solution for 14 days. For implant stability, the change in the pH of the solution is a critical parameter. The pH of the bare Mg alloy samples increased from 7.4 pH (the initial) to 8.58 within one day. After 14 days, the pH of the Mg alloy was observed to be 10.15. However, in the case of the coated samples Sr-D-Ca-P and Sr-D-Ca-P/PLLA-HAp, the pH change after 14 days was noted to be 8.72 and 8.12, respectively. The results indicate that bare Mg samples showed more corrosion as compared to the coated samples (Fig. 3a). Sr-D-Ca-P/PLLA-HAp coated samples displayed a lowered pH as compared to the Sr-D-Ca-P coated samples, which can also be attributed to the PLLA degradation products which are acidic in nature hence lowering the pH [47].

The hydrogen gas evolution showed the same tendency. As compared to the coated samples, bare Mg alloy showed a greater release of hydrogen gas (Fig. 3b). In the case of the coated samples, the hydrogen gas evolution was drastically decreased. Sr-D-Ca-P and Sr-D-Ca-P/PLLA-HAp coated samples showed an exceptionally low release of hydrogen gas even after 14 days indicating that the coatings successfully decreased the degradation of the Mg alloy. The higher release of the hydrogen gas by Mg samples indicated a greater rate of corrosion. The pH change and hydrogen gas results indicate that the coating efficiently protected the Mg alloy surface from the penetration of fluids.

The weight loss of Mg, Sr-D-Ca-P, and Sr-D-Ca-P/PLLA-HAp coated samples is displayed in (Fig. 3c). Over time, the degradation rate for all the samples increased. However, it can be observed that the weight loss was low for the coated samples, as compared to the bare Mg sample at all the time points. After the 14 days of immersion, the average weight loss for Mg, Sr-D-Ca-P, and Sr-D-Ca-P/PLLA-HAp coated samples was 20.9 ±

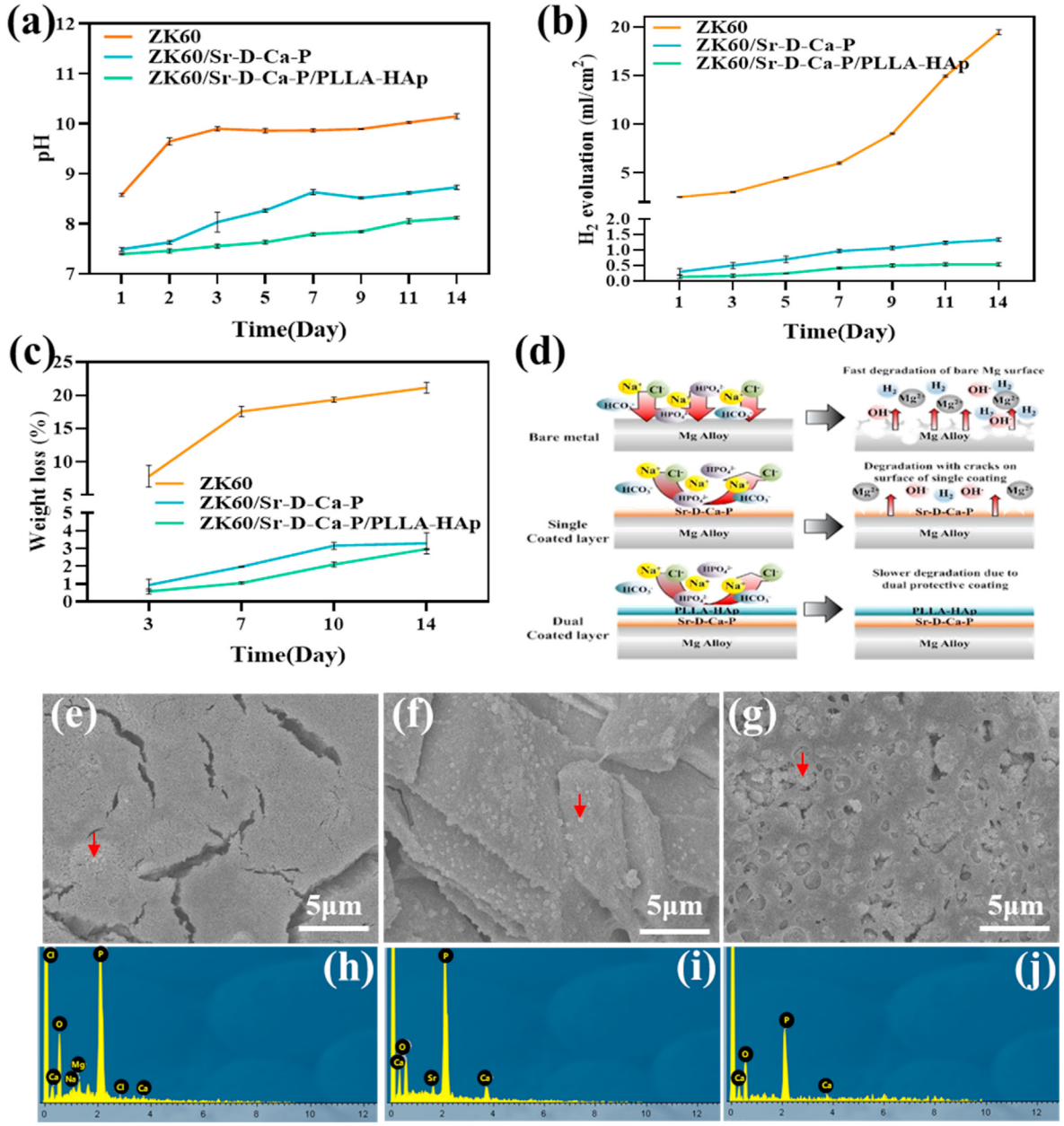

Fig. 3. (a) Ph change, (b) H_2 evolution, and (c) weight loss rate in Hank's solution, (d) schematic representation of degradation process of ZK60, ZK60/Sr-D-Ca-P, and ZK60/Sr-D-Ca-P/PLLA-HAp coated samples. SEM observation of apatite formation on the surfaces of (e) ZK60, (f) ZK60/Sr-D-Ca-P, and (g) ZK60/Sr-D-Ca-P/PLLA-HAp along with EDS analysis for corresponding samples (h) ZK60, (i) ZK60/Sr-D-Ca-P, and (j) ZK60/Sr-D-Ca-P/PLLA-HAp.

0.83%, 3.2 ± 0.59%, and 2.9 ± 0.02%, respectively. The weight loss in the first 3 days can be attributed to exposure of a larger surface area of Mg to the solution, which in turn aided the exothermic reactions [48]. This factor facilitates the corrosion rate. In the beginning, the higher salt concentration also contributes to the rapid corrosion, but as time passes a protective corrosion layer is formed declining the degradation rate in later stages. The protective Sr-D-Ca-P and Sr-D-Ca-P/PLLA-HAp coatings improved the degree of Mg alloy degradation. In the case of Sr-D-Ca-P coating, the incorporation of Sr into the Ca and P might inhibit the coating dissolution. For Sr-D-Ca-P/PLLA-HAp samples, the degradation rate is further decreased, which can be attributed to the fact that HAp incorporated PLLA formed strong adhesion with the inorganic Sr-D-Ca-P coating. The results of the degradation rate are well coherent with the pH change and the hydrogen gas evolution.

The corrosion of the Mg metal can be explained with the following reaction scheme [2].

$$Mg = Mg^{2+} + 2e^{-} \ (\text{Anode}) \quad (1)$$

$$2H_2O + 2e^{-} = H_2 + 2OH^{-} \ (\text{Cathode}) \quad (2)$$

$$Mg^{2+} + 2H_2O = Mg(OH)_2 + H_2 (\text{Overall reaction}) \quad (3)$$

Corrosion of Mg takes place by the conversion of Mg into magnesium hydroxide ($Mg(OH)_2$) with the continuous release of the H_2 gas (Eq. (3)). Different ions present in the solution such as $CO^{2-}{}_3$, $PO^{3-}{}_4$, and Cl^{-} are attracted by the surface. Magnesium hydroxide is itself insoluble in the solution, but as the concentration of the Cl^{-} ions increases it is converted into soluble $MgCl_2$. With this dissolution the corrosion rate of the Mg surface increases [49]. Previous results indicate that Ca and P coating decreased the degradation rate [50,51]. The incorporation of Sr into Ca and P further reduces the degradation rate of Mg [20]. The results suggest that the first inorganic coating effectively lowers the rate of degradation. However, the gaps generated between the coating and metal surface allow the ions in the solution to penetrate the coating. As these ions reach the surface of the coating, the conversion of Mg ions to $(Mg(OH)_2)$ is accelerated.

With the addition of HAp particles incorporated in PLLA, the gaps are filled providing a shield against the movement of the ions to the metal surface. This helps to further reduce the rate of degradation along with enhanced biocompatibility because of the incorporation of HAp particles in the polymer. PLLA polymer has a higher ratio of oxygen atoms in its chemical structure which promote electrostatic forces between that polymer and the attachment surface (Sr-D-Ca-P) [34]. The strong adhesion between the inorganic Sr-D-Ca-P layer and the organic polymer layer (incorporated with HAp) consequently provides stronger protection against the fast corrosion of the metal.

In vitro apatite formation is one of the ways to evaluate the osteointegration ability of the implants. Mg, Sr-D-Ca-P, and Sr-D-Ca-P/PLLA-HAp coated samples were immersed in SBF (stimulated body fluid), to evaluate the *in vitro* bioactivity. The agglomerated white particles on the surface of the Sr-D-Ca-P, and Sr-D-Ca-P/PLLA-HAp coated samples were an indication that apatite formation occurred (Fig. 3e–g, Cross-sectional image Fig. S3). This is also supported by the elemental analysis by EDS (Fig. 3h–j). Bare Mg alloy EDS analysis showed C, O, Na, Cl, Ca, and P. This indicates the formation of $Mg(OH)_2$, $MgCl_2$, Ca-rich (e.g. $Ca_x(PO_4)_y$) and Na-rich corrosion products on the surface of corroded bare Mg alloy [52]. It has been previously reported that Sr-D-Ca-P coated samples showed apatite formation when immersed in SBF for 14 days [27]. For the polymer-coated samples, due to the lack of Ca and P particles on the outer surface, the apatite formation is slowed down. For the dual Sr-D-Ca-P/PLLA-HAp coating, the outer PLLA protective layer is incorporated with the HAp particles. The slow release of the HAp particles from the outer PLLA layer supported the apatite formation in the case of the Sr-D-Ca-P/PLLA-HAp coated samples.

3.3. In vitro biocompatibility

The biocompatibility of the Mg, Sr-D-Ca-P, and Sr-D-Ca-P/PLLA-HAp coated samples was evaluated by cell viability and cell proliferation of the pre-osteoblast MC3T3-E1 cells. The implant morphology plays a vital role in cell behavior. For the bare Mg alloy, the rapid change in the pH and the fast degeneration affects the cell's growth [17,51]. For this reason, we compared the Sr-D-Ca-P, and Sr-D-Ca-P/PLLA-HAp coated samples with control.

Cell viability results of the Sr-D-Ca-P and Sr-D-Ca-P/PLLA-HAp coated samples via direct method indicated that both types of coatings were biocompatible (Fig. 4a). Sr-D-Ca-P/PLLA-HAp coated samples showed cell viability compared to the control suggesting that incorporation of the HAp particles supported cell growth by increasing the biocompatibility.

The growth of the bone tissues supported by the implant can be determined by the cell proliferation behavior [17]. The cell proliferation on the Sr-D-Ca-P and Sr-D-Ca-P/PLLA-HAp coated samples, as compared to the control, are shown in (Fig. 4b). Confocal images after 1, 3, and 7 days of the incubation period showed active cell spreading and growth on both coated samples. Sr-D-Ca-P coating has been previously reported to have excellent effects on cell growth and cell proliferation due to the favorable effect inserted by Ca, Mg, and Sr ions on the cells [26]. The Sr-D-Ca-P/PLLA-HAp coated samples showed excellent cell proliferation compared to the control. The enhancement in the Sr-D-Ca-P/PLLA-HAp biocompatibility as compared to the Sr-D-Ca-P only coating can be assorted to the HAp particles and PLLA. The PLLA and HAp particles have been shown to have excellent biocompatibility [42,53]. Thus, the combined effect of the Sr-D-Ca-P and PLLA-HAp coating resulted in exceptional cell proliferation. Based on the same concept that the coating surfaces decrease the degradation rate; it also contributes to the cell proliferation behavior. In the highly corrosive environment, due to the abundant release of Mg ions, high pH, and hydrogen gas evolution, cytotoxicity leads to cell death [54]. Sr-D-Ca-P and Sr-D-Ca-P/PLLA-HAp coated surfaces decreased the degradation rate, which flourishes the cell growth due to a favorable environment. The cell proliferation study implies that Sr-D-Ca-P/PLLA-HAp is a non-toxic coating with excellent biocompatibility.

3.4. In vitro osteogenic property

The effect of the Mg, Sr-D-Ca-P, and Sr-D-Ca-P/PLLA-HAp coated samples on the osteogenic differentiation was determined by the expression of alkaline phosphatase (ALP), osteopontin (OPN), and osteocalcin (OCN) through q-PCR (Fig. 4c–e). Bone mineralization can be determined by the ALP enzyme, OPN, and OCN are non-collagenous proteins located in the mineralized tissues [19,55]. ALP is a marker for the earliest stage of an early osteoblastic cells. OPN is known to be involved in the cell attachment to the extracellular matrix by regulating the growth of hydroxyapatite crystals within the bone matrix [56]. It is an early-stage marker as compared to OCN which is considered a late-stage marker. OCN protein is among the most abundant non-collagenous proteins observed in bones. The ALP expression for Mg alloy samples was higher as compared to the other two samples in the day 14 results. This could be attributed to the release of Mg and Zn ions from the degradation of the Mg alloy. It has been reported that Mg and Zn ions promote the ALP expression [57]. Sr-D-Ca-P/PLLA-HAp coated samples showed high expressions for OCN and OPN at all time points. The results from the q-PCR analysis suggest that Sr-D-Ca-P/PLLA-HAp coated samples were highly suitable for bone regeneration.

3.5. In vivo degradation and biocompatibility

3.5.1. Micro CT scan

The fast degradation of the Mg alloy-based implants results in gaps between the implant interface and the surroundings. For orthopedic

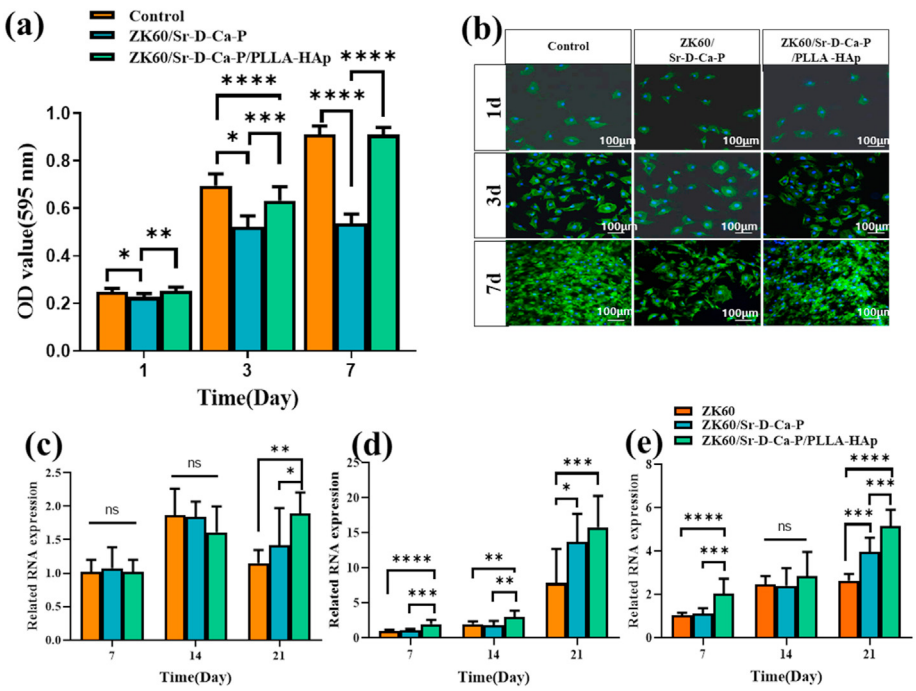

Fig. 4. (a) *In vitro* cell viability test (*p < 0.1) (**p < 0.01) (***p < 0.001) (****p < 0.0001), and (b) observation by confocal microscopy of cell proliferation. MC3T3E1 cells were used for the cell viability test. Related gene expressions of (c) ALP, (d) OPN, and (e) OCN on the ZK60, ZK60/Sr-D-Ca-P, ZK60/Sr-D-Ca-P/PLLA-HAp for 3 weeks (n.s: not significant) (*p < 0.1) (**p < 0.01) (***p < 0.001) (****p < 0.0001).

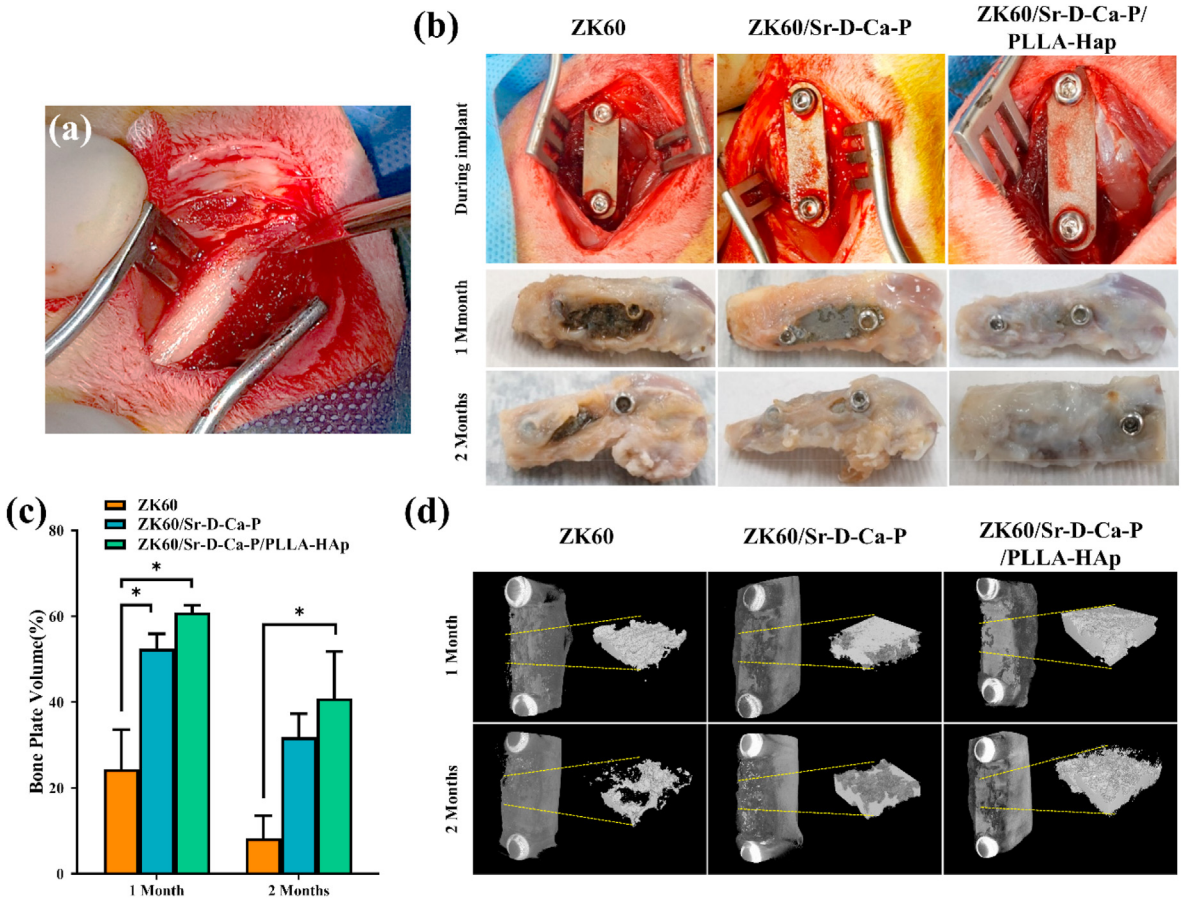

Fig. 5. (a, b) *In vivo* implantation of the bone plate on rabbit model, (c) percentage of remaining bone plate (*p < 0.1), and (d) micro-CT 3D visualized image.

implants, such as bone plates, corrosion resistance is a vital factor. To evaluate the degradation of Mg, Sr-D-Ca-P, and Sr-D-Ca-P/PLLA-HAp coated samples, an *in vivo* study was conducted. All three samples were implanted on the femur of the rabbit in the form of a bone plate attached to the bone by screws. Fig. 5b shows the implantation of a bone plate and extracted samples after one and two months. During implantation, none of the samples showed any effect of interaction with the blood or the bones.

To evaluate the implant degradation after 1 and 2 months, micro-computed tomography (microCT) was used. Fig. 5d shows the micro-CT scan images of the Mg, Sr-D-Ca-P, and Sr-D-Ca-P/PLLA-HAp coated samples after 1 and 2 months of implantation. The images clearly exhibit that degradation of the bare Mg alloy sample was more as compared to the coated samples. Among the coated samples, Sr-D-Ca-P/PLLA-HAp showed lesser degradation after 2 months of implantation as compared to the Sr-D-Ca-P coated samples. The volume reduction of the implants from the micro-CT scan analysis for Mg, Sr-D-Ca-P, and Sr-D-Ca-P/PLLA-HAp coated bone plates were 8.2 ± 5.3%, 31.8 ± 5.4%, and 40.8 ± 10.9% respectively, after 2 months of implantation (Fig. 5c). These results imply that Sr-D-Ca-P/PLLA-HAp coating protected the Mg from the fast degradation *in vivo*. The corrosion resistance effect of the dual coating was clearly seen in the *in vivo* results. Therefore, Sr-D-Ca-P/PLLA-

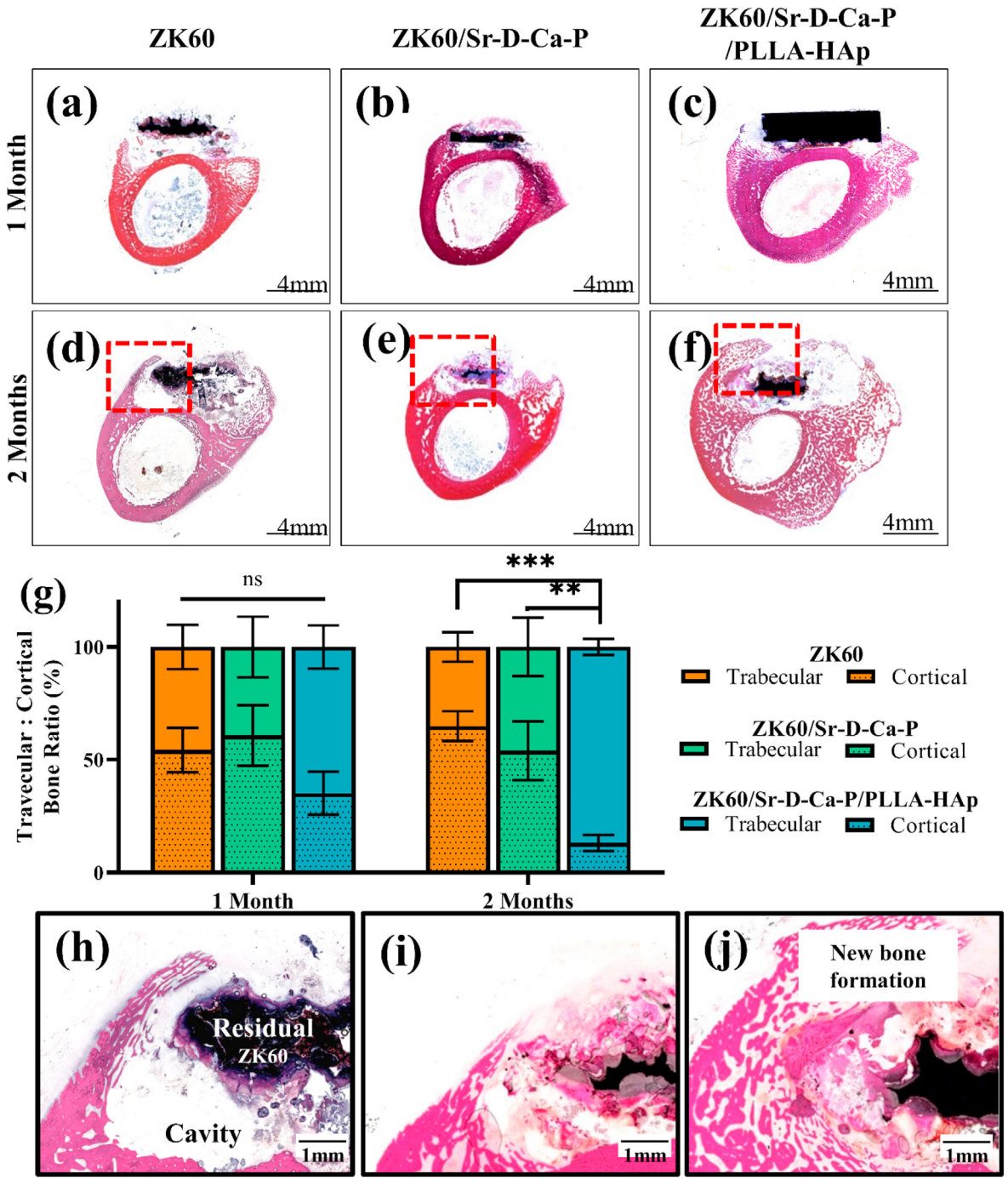

Fig. 6. Histological evaluation of *in vivo* implantation for (a, b, c) 1 and (d, e, f) 2 months; (a, d) ZK60 bone plate, (b, e) ZK60/Sr-D-Ca-P coated bone plate, and (c, f) ZK60/Sr-D-Ca-P/PLLA-HAp bone plate, (g) quantitative ratio between the trabecular and cortical bone (n.s: not significant) (**$p < 0.01$) (***$p < 0.001$). Histological evaluation of interface of (h) ZK60 bone plate, (i) ZK60/Sr-D-Ca-P bone plate, and (j) ZK60/Sr-D-Ca-P/PLLA-HAp bone plate implanted after 2 months.

HAp coating on Mg alloy is a promising strategy for application in bone plates; Sr-D-Ca-P/PLLA-HAp coated bone plates can provide ample support to regenerate the fractured bone.

3.5.2. Histological analysis

To evaluate the response of the Mg, Sr-D-Ca-P, and Sr-D-Ca-P/PLLA-HAp coated bone plates on the tissues after implantation, histological analysis was performed (Fig. 6). For the Mg and Sr-D-Ca-P coated bone plates, cavities and gaps are detected on the interfaces (Fig. 6a,b,d,e). Due to the fast degradation process, hydrogen gas is released from the Mg-based bone implants. The evolution of the hydrogen gas might have separated the surface of Mg and Sr-D-Ca-P coated bone plates from the tissue layer. Sr-D-Ca-P/PLLA-HAp coated bone plates showed good osteointegration, as inflammation and interface loosening are not observed in these samples (Fig. 6c,f). It is observed that Sr-D-Ca-P/PLLA-HAp coated bone plates showed extraordinary bone growth compared to bare Mg and Sr-D-Ca-P coated bone plates after 2 months of implantation. Fig. 6g represent the quantitative analysis of the ratio between the trabecular bone and cortical bone. After 1 and 2 months of the bone plate implantation the cortical bone is surrounded by the trabecular bone in all the samples, but the formation of the trabecular bone is highest in Sr-D-Ca-P/PLLA-HAp coated bone plate samples.

The histological stained samples showed that after two months, Sr-D-Ca-P/PLLA-HAp coated bone plate was surrounded by new bone (Fig. 6j). Whereas the bare Mg alloy plate created large cavities surrounding the bone (Fig. 6h). Sr-D-Ca-P coated bone plate showed fewer cavities in the surrounding, but the negligible new bone formation was observed (Fig. 6i).

The reduced degradation rate means that the release of the Mg ions is also decreased. Mg ions protect the excessive bone resorption [58], but the higher concentration of the Mg ion is not favorable for the bone formation process. The Mg substituted apatite inhibits the extracellular matrix formation, resulting in a toxic effect on the bone cells [59,60]. Mg ions tend to bind to the pyrophosphate resulting in insoluble salts, inhibiting hydroxy apatite crystal formation [60]. The fact that Sr-D-Ca-P and Sr-D-Ca-P/PLLA-HAp coated bone plates showed greater bone formation than uncoated Mg bone plates is directly related to the fast release of Mg ions. Moreover, the release of the HAp from the PLLA-HAp layer offers abundant phosphate and calcium ions, which help in the precipitation of the bone-like apatite crystals [61]. The slower degradation and the release of the HAp particles along with Sr ions had a collective effect on the remarkable bone formation of the Sr-D-Ca-P/PLLA-HAp coated bone plate. The *in vivo* results imply that Sr-D-Ca-P/PLLA-HAp coated bone plate is also highly suitable for osteoporosis patients, as it is a rich source of Ca and P ions, which can help strengthen the weak bones. For the biodegradable implants, with the passage of time the degradation is inevitable. As the process of implant degradation takes place, the fracture site can be weakened. However, the weakening of the fracture site can be compensated with bone remodeling phenomena. Our *in vivo* findings support this hypothesis, that Sr-D-Ca-P/PLLA-HAp coated implanted bone plate not only slowed the degradation rate but also enhanced the new bone formation.

Fig. 7 represents the hypothetical mechanism that contributed to the remarkable bone regeneration of the dual Sr-D-Ca-P/PLLA-HAp coated bone plate. The dual coating protected the inner surface from the damage caused by the outer ion-rich environment. The gradual release of the Ca and P ions from the PLLA resulted in enhanced biocompatibility. As the degradation progresses, Ca, Sr, and P ions are released from the coating surface with a slow release of Mg ions from the metal surface. Mg ions activate the MAPK/ERK and Wnt signal pathways which trigger the osteogenic differentiation [62].

The study results proved our hypothesis, that Sr-D-Ca-P inner coating PLLA incorporated with HAp protective layering will decrease the degradation time and increase the biocompatibility of the bone plate. Sr-D-Ca-P/PLLA-HAp coating not only protected against degradation but also enhanced the biocompatibility, which is evident through the remarkable bone formation by Sr-D-Ca-P/PLLA-HAp coated bone plate. The remodeling phenomenon displayed by Sr-D-Ca-P/PLLA-HAp coated bone plate has not been reported so far to the best of our knowledge. The approach that slows degradation of the bone plate is compensated by the new bone formation and opens a new facet in the field of orthopedic regenerative biomaterials. The simplicity of the preparation procedure for the dual coating, remarkable bone formation, and protection against degradation renders our system suitable for application on a wider scale.

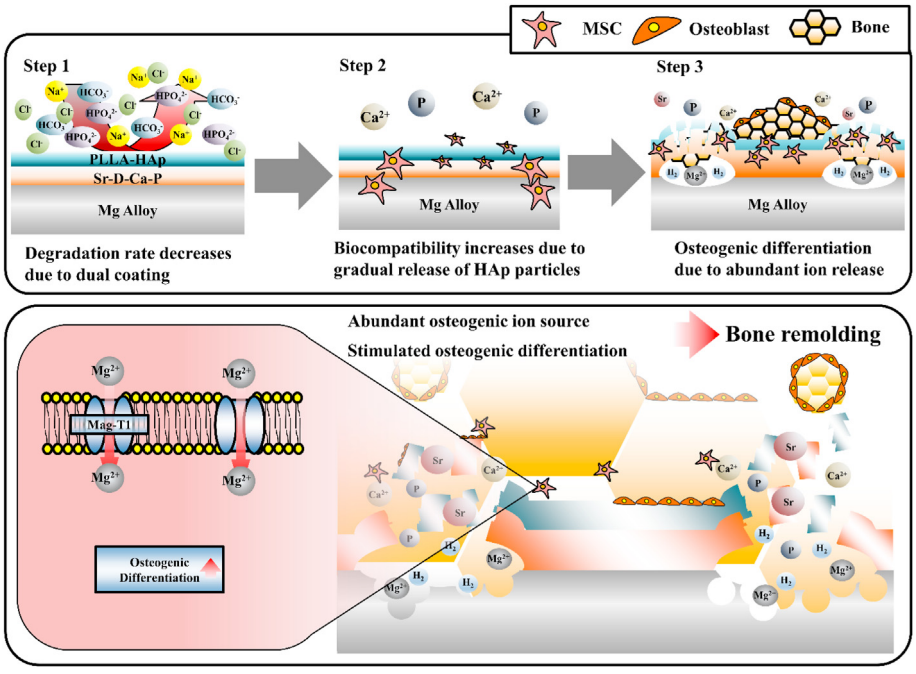

Fig. 7. Illustration representing the mechanism of bone regeneration due to dual Sr-D-Ca-P/PLLA-HAp coating the Mg alloy bone plate.

4. Conclusion

The Sr-D-Ca-P/PLLA-HAp coating was developed on Mg alloy by chemical immersion and dip-coating procedure. Sr-D-Ca-P/PLLA-HAp coating successfully resisted the fast degradation of the Mg alloy, in comparison to the pristine Mg alloy and Sr-D-Ca-P single coating. The degradation resistance of the dual coating also increased its biocompatibility. With an increase in cell proliferation, osteogenic marker expressions for MC3T3-E1 cells were enhanced. *In vivo* results suggested that dual Sr-D-Ca-P/PLLA-HAp coated bone plate resisted the *in vivo* degradation, while bone formation dramatically increased after two months of implantation in a rabbit model. As compared to bare Mg alloy and Sr-D-Ca-P coated bone plates, dual Sr-D-Ca-P/PLLA-HAp coated bone plates showed superior bone remodeling. To the best of our knowledge, bone remodeling displayed by Sr-D-Ca-P/PLLA-HAp coated bone plates has been reported for the first time opening new aspects in the regenerative biomaterial field. The results demonstrate that dual Sr-D-Ca-P/PLLA-HAp coating on Mg alloy for bone implants is an excellent strategy for enhanced bone regeneration and controllable degradation.

Credit author statement

Seong-Su Park: Conceptualization, Methodology, Data Curation, Investigation, Writing - original draft. **Ume Farwa**: Methodology, Investigation, Writing - original draft, Writing - Review & Editing. **Ihho Park**: Investigation, Formal analysis. **Byoung-Gi Moon**: Investigation, Formal analysis. **Soo-Bin Im:** Formal analysis. **Byong-Taek Lee**: Conceptualization, Supervision, Funding acquisition, Writing - Review & Editing, Project Administration, Resources.

Declaration of competing interest

The authors declare that they have no known competing financial interests or personal relationships that could have appeared to influence the work reported in this paper.

Data availability

The authors do not have permission to share data.

Acknowledgement

The research was funded by the National Research Foundation of Korea (NRF) funded by the Ministry of Education, (2015R1A6A1A03032522), South Korea, and partially by Soonchunhyang University, South Korea.

Appendix A. Supplementary data

Supplementary data to this article can be found online at https://doi.org/10.1016/j.mtbio.2022.100533.

References

[1] B. Beale, Orthopedic clinical techniques femur fracture repair, Clin. Tech. Small Anim. Pract. 19 (2004) 134–150.
[2] M.P. Staiger, A.M. Pietak, J. Huadmai, G. Dias, Magnesium and its alloys as orthopedic biomaterials: a review, Biomaterials 27 (2006) 1728–1734.
[3] C. Seal, K. Vince, M. Hodgson, Biodegradable surgical implants based on magnesium alloys–A review of current research, in: IOP Conference Series: Materials Science and Engineering, IOP Publishing, 2009, 012011.
[4] H.R. Bakhsheshi-Rad, A.F. Ismail, M. Aziz, M. Akbari, Z. Hadisi, S.M. Khoshnava, E. Pagan, X. Chen, Co-incorporation of graphene oxide/silver nanoparticle into poly-L-lactic acid fibrous: a route toward the development of cytocompatible and antibacterial coating layer on magnesium implants, Mater. Sci. Eng. C 111 (2020), 110812.
[5] C. Wang, B. Zhang, S. Yu, H. Zhang, W. Zhou, R. Luo, Y. Wang, W. Bian, G. Mao, Incorporation of Mg-phenolic networks as a protective coating for magnesium alloy to enhance corrosion resistance and osteogenesis in vivo, J. Magnes. Alloy. (2022), https://doi.org/10.1016/j.jma.2022.03.010.
[6] Y. Hou, X. Zhang, J. Li, L. Wang, S. Guan, A multi-functional MgF2/polydopamine/hyaluronan-astaxanthin coating on the biodegradable ZE21B alloy with better corrosion resistance and biocompatibility for cardiovascular application, J. Magnes. Alloy. (2022), https://doi.org/10.1016/j.jma.2022.06.008.
[7] S. Hiromoto, E. Nozoe, K. Hanada, T. Yoshimura, K. Shima, T. Kibe, N. Nakamura, K. Doi, In vivo degradation and bone formation behaviors of hydroxyapatite-coated Mg alloys in rat femur, Mater. Sci. Eng. C 122 (2021), 111942.
[8] Y. Xin, T. Hu, P. Chu, In vitro studies of biomedical magnesium alloys in a simulated physiological environment: a review, Acta Biomater. 7 (2011) 1452–1459.
[9] L. Li, M. Zhang, Y. Li, J. Zhao, L. Qin, Y. Lai, Corrosion and biocompatibility improvement of magnesium-based alloys as bone implant materials: a review, Regenerative biomaterials 4 (2017) 129–137.
[10] H. Hornberger, S. Virtanen, A.R. Boccaccini, Biomedical coatings on magnesium alloys–a review, Acta Biomater. 8 (2012) 2442–2455.
[11] X. Yang, M. Li, X. Lin, L. Tan, G. Lan, L. Li, Q. Yin, H. Xia, Y. Zhang, K. Yang, Enhanced in vitro biocompatibility/bioactivity of biodegradable Mg–Zn–Zr alloy by micro-arc oxidation coating contained Mg2SiO4, Surf. Coating. Technol. 233 (2013) 65–73.
[12] M. Wu, F. Chen, H. Liu, P. Wu, Z. Yang, Z. Zhang, J. Su, L. Cai, Y. Zhang, Bioinspired sandwich-like hybrid surface functionalized scaffold capable of regulating osteogenesis, angiogenesis, and osteoclastogenesis for robust bone regeneration, Materials Today Bio (2022), 100458.
[13] S. Shadanbaz, G.J. Dias, Calcium phosphate coatings on magnesium alloys for biomedical applications: a review, Acta Biomater. 8 (2012) 20–30.
[14] Y. Zhao, D. Guo, S. Hou, H. Zhong, J. Yan, C. Zhang, Y. Zhou, Porous allograft bone scaffolds: doping with strontium, PLoS One 8 (2013), e69339.
[15] D.d.S. Tavares, C.X. Resende, M.P. Quitan, L.d.O. Castro, J.M. Granjeiro, G.d.A. Soares, Incorporation of strontium up to 5 Mol.(%) to hydroxyapatite did not affect its cytocompatibility, Mater. Res. 14 (2011) 456–460.
[16] Y. Huang, Q. Ding, X. Pang, S. Han, Y. Yan, Corrosion behavior and biocompatibility of strontium and fluorine co-doped electrodeposited hydroxyapatite coatings, Appl. Surf. Sci. 282 (2013) 456–462.
[17] X.B. Chen, D.R. Nisbet, R.W. Li, P. Smith, T.B. Abbott, M.A. Easton, D.-H. Zhang, N. Birbilis, Controlling initial biodegradation of magnesium by a biocompatible strontium phosphate conversion coating, Acta Biomater. 10 (2014) 1463–1474.
[18] X. Gu, X. Xie, N. Li, Y. Zheng, L. Qin, In vitro and in vivo studies on a Mg–Sr binary alloy system developed as a new kind of biodegradable metal, Acta Biomater. 8 (2012) 2360–2374.
[19] S.S. Singh, A. Roy, B.E. Lee, J. Ohodnicki, A. Loghmanian, I. Banerjee, P.N. Kumta, A study of strontium doped calcium phosphate coatings on AZ31, Mater. Sci. Eng. C 40 (2014) 357–365.
[20] Y. Lu, L. Tan, B. Zhang, J. Lin, K. Yang, Synthesis and characterization of Ca–Sr–P coating on pure magnesium for biomedical application, Ceram. Int. 40 (2014) 4559–4565.
[21] C. Lindahl, S. Pujari-Palmer, A. Hoess, M. Ott, H. Engqvist, W. Xia, The influence of Sr content in calcium phosphate coatings, Mater. Sci. Eng. C 53 (2015) 322–330.
[22] D. Gopi, N. Murugan, S. Ramya, E. Shinyjoy, L. Kavitha, Ball flower like manganese, strontium substituted hydroxyapatite/cerium oxide dual coatings on the AZ91 Mg alloy with improved bioactive and corrosion resistance properties for implant applications, RSC Adv. 5 (2015) 27402–27411.
[23] D. Gopi, N. Murugan, S. Ramya, L. Kavitha, Electrodeposition of a porous strontium-substituted hydroxyapatite/zinc oxide duplex layer on AZ91 magnesium alloy for orthopedic applications, J. Mater. Chem. B 2 (2014) 5531–5540.
[24] Y. Lu, P. Wan, L. Tan, B. Zhang, K. Yang, J. Lin, Preliminary study on a bioactive Sr containing Ca–P coating on pure magnesium by a two-step procedure, Surf. Coating. Technol. 252 (2014) 79–86.
[25] N. Yu, S. Cai, F. Wang, F. Zhang, R. Ling, Y. Li, Y. Jiang, G. Xu, Microwave assisted deposition of strontium doped hydroxyapatite coating on AZ31 magnesium alloy with enhanced mineralization ability and corrosion resistance, Ceram. Int. 43 (2017) 2495–2503.
[26] J. Han, P. Wan, Y. Sun, Z. Liu, X. Fan, L. Tan, K. Yang, Fabrication and evaluation of a bioactive Sr–Ca–P contained micro-arc oxidation coating on magnesium strontium alloy for bone repair application, J. Mater. Sci. Technol. 32 (2016) 233–244.
[27] P. Makkar, H.J. Kang, A.R. Padalhin, O. Faruq, B. Lee, In-vitro and in-vivo evaluation of strontium doped calcium phosphate coatings on biodegradable magnesium alloy for bone applications, Appl. Surf. Sci. 510 (2020), 145333.
[28] K.A. Khalil, S.W. Kim, N. Dharmaraj, K.W. Kim, H.Y. Kim, Novel mechanism to improve toughness of the hydroxyapatite bioceramics using high-frequency induction heat sintering, J. Mater. Process. Technol. 187 (2007) 417–420.
[29] N.A. Barakat, K. Khalil, F.A. Sheikh, A. Omran, B. Gaihre, S.M. Khil, H.Y. Kim, Physiochemical characterizations of hydroxyapatite extracted from bovine bones by three different methods: extraction of biologically desirable HAp, Mater. Sci. Eng. C 28 (2008) 1381–1387.
[30] D.-Y. Lin, X.-X. Wang, Preparation of hydroxyapatite coating on smooth implant surface by electrodeposition, Ceram. Int. 37 (2011) 403–406.
[31] M. Diez, M.-H. Kang, S.-M. Kim, H.-E. Kim, J. Song, Hydroxyapatite (HA)/poly-L-lactic acid (PLLA) dual coating on magnesium alloy under deformation for biomedical applications, J. Mater. Sci. Mater. Med. 27 (2016) 1–9.
[32] S.-M. Kim, M.-H. Kang, H.-E. Kim, H.-K. Lim, S.-H. Byun, J.-H. Lee, S.-M. Lee, Innovative micro-textured hydroxyapatite and poly (l-lactic)-acid polymer composite film as a flexible, corrosion resistant, biocompatible, and bioactive coating for Mg implants, Mater. Sci. Eng. C 81 (2017) 97–103.
[33] Y.F. Zheng, X.N. Gu, F. Witte, Biodegradable metals, Mater. Sci. Eng. R Rep. 77 (2014) 1–34.

[34] L. Xu, A. Yamamoto, Characteristics and cytocompatibility of biodegradable polymer film on magnesium by spin coating, Colloids Surf. B Biointerfaces 93 (2012) 67–74.
[35] Z. Huan, M. Leeflang, J. Zhou, L. Fratila-Apachitei, J. Duszczyk, In vitro degradation behavior and cytocompatibility of Mg–Zn–Zr alloys, J. Mater. Sci. Mater. Med. 21 (2010) 2623–2635.
[36] Y. Pan, C. Chen, D. Wang, Z. Lin, Preparation and bioactivity of micro-arc oxidized calcium phosphate coatings, Mater. Chem. Phys. 141 (2013) 842–849.
[37] H. Watanabe, K. Moriwaki, T. Mukai, T. Ohsuna, K. Hiraga, K. Higashi, Materials processing for structural stability in a ZK60 magnesium alloy, Mater. Trans. 44 (2003) 775–781.
[38] J.-K. Han, H.-Y. Song, F. Saito, B.-T. Lee, Synthesis of high purity nano-sized hydroxyapatite powder by microwave-hydrothermal method, Mater. Chem. Phys. 99 (2006) 235–239.
[39] Y. Sasikumar, M. Solomon, L. Olasunkanmi, E. Ebenso, Effect of surface treatment on the bioactivity and electrochemical behavior of magnesium alloys in simulated body fluid, Mater. Corros. 68 (2017) 776–790.
[40] S.-R. Wang, W. Min, S.-B. Kang, J.-H. Cho, Microstructure comparison of ZK60 alloy under casting, twin roll casting and hot compression, Trans. Nonferrous Metals Soc. China 20 (2010) 763–768.
[41] H.M. Wong, K.W. Yeung, K.O. Lam, V. Tam, P.K. Chu, K.D. Luk, K.M. Cheung, A biodegradable polymer-based coating to control the performance of magnesium alloy orthopaedic implants, Biomaterials 31 (2010) 2084–2096.
[42] A. Abdal-hay, N.A. Barakat, J.K. Lim, Hydroxyapatite-doped poly (lactic acid) porous film coating for enhanced bioactivity and corrosion behavior of AZ31 Mg alloy for orthopedic applications, Ceram. Int. 39 (2013) 183–195.
[43] K. Huang, S. Cai, G. Xu, M. Ren, X. Wang, R. Zhang, S. Niu, H. Zhao, Sol–gel derived mesoporous 58S bioactive glass coatings on AZ31 magnesium alloy and in vitro degradation behavior, Surf. Coating. Technol. 240 (2014) 137–144.
[44] A. Zomorodian, C. Santos, M. Carmezim, T.M. e Silva, J. Fernandes, M.d.F. Montemor, In-vitro" corrosion behaviour of the magnesium alloy with Al and Zn (AZ31) protected with a biodegradable polycaprolactone coating loaded with hydroxyapatite and cephalexin, Electrochim. Acta 179 (2015) 431–440.
[45] P. Amaravathy, T.S. Kumar, Bioactivity enhancement by Sr doped Zn-Ca-P coatings on biomedical magnesium alloy, J. Magnes. Alloy. 7 (2019) 584–596.
[46] K. Chiu, M. Wong, F. Cheng, H.C. Man, Characterization and corrosion studies of fluoride conversion coating on degradable Mg implants, Surf. Coating. Technol. 202 (2007) 590–598.
[47] R.-C. Zeng, L.-y. Cui, K. Jiang, R. Liu, B.-D. Zhao, Y.-F. Zheng, In vitro corrosion and cytocompatibility of a microarc oxidation coating and poly (l-lactic acid) composite coating on Mg–1Li–1Ca alloy for orthopedic implants, ACS Appl. Mater. Interfaces 8 (2016) 10014–10028.
[48] X.-M. Wang, G.-J. Lu, L.-Y. Cui, C.-B. Liu, M.B. Kannan, F. Zhang, S.-Q. Li, Y.-H. Zou, R.-C. Zeng, In Vitro Degradation and Biocompatibility of Vitamin C Loaded Ca-P Coating on a Magnesium Alloy for Bioimplant Applications, Corrosion Communications, 2022.
[49] J. Niu, G. Yuan, Y. Liao, L. Mao, J. Zhang, Y. Wang, F. Huang, Y. Jiang, Y. He, W. Ding, Enhanced biocorrosion resistance and biocompatibility of degradable Mg–Nd–Zn–Zr alloy by brushite coating, Mater. Sci. Eng. C 33 (2013) 4833–4841.
[50] Y. Wang, Z. Zhu, X. Xu, Y. He, B. Zhang, Improved corrosion resistance and biocompatibility of a calcium phosphate coating on a magnesium alloy for orthopedic applications, Eur. J. Inflamm. 14 (2016) 169–183.
[51] X. Xiao, Q.-s. Zhu, Y.-c. Su, G.-y. Li, In vitro degradation and biocompatibility of Ca-P coated magnesium alloy, Chem. Res. Chin. Univ. 29 (2013) 285–289.
[52] J. Gonzalez, R.Q. Hou, E.P. Nidadavolu, R. Willumeit-Römer, F. Feyerabend, Magnesium degradation under physiological conditions–best practice, Bioact. Mater. 3 (2018) 174–185.
[53] S. Ramesh, C. Tan, W. Yeo, R. Tolouei, M. Amiriyan, I. Sopyan, W. Teng, Effects of bismuth oxide on the sinterability of hydroxyapatite, Ceram. Int. 37 (2011) 599–606.
[54] P. Xiong, Z. Jia, M. Li, W. Zhou, J. Yan, Y. Wu, Y. Cheng, Y. Zheng, Biomimetic Ca, Sr/P-doped silk fibroin films on Mg-1Ca alloy with dramatic corrosion resistance and osteogenic activities, ACS Biomater. Sci. Eng. 4 (2018) 3163–3176.
[55] N. Stephanie, H. Katarina, L.R. Amir, H.A. Gunawan, ALP gene expression in cDNA samples from bone tissue engineering using a HA/TCP/Chitosan scaffold, in: Journal of Physics: Conference Series, IOP Publishing, 2017, 012112.
[56] J. Sodek, B. Ganss, M. McKee, Osteopontin, Critical Reviews in Oral Biology & Medicine 11 (2000) 279–303.
[57] K. Sorimachi, Activation of alkaline phosphatase with Mg2+ and Zn2+ in rat hepatoma cells. Accumulation of apoenzyme, J. Biol. Chem. 262 (1987) 1535–1541.
[58] C. Janning, E. Willbold, C. Vogt, J. Nellesen, A. Meyer-Lindenberg, H. Windhagen, F. Thorey, F. Witte, Magnesium hydroxide temporarily enhancing osteoblast activity and decreasing the osteoclast number in peri-implant bone remodelling, Acta Biomater. 6 (2010) 1861–1868.
[59] Y.-K. Kim, K.-B. Lee, S.-Y. Kim, Y.-S. Jang, J.H. Kim, M.-H. Lee, Improvement of osteogenesis by a uniform PCL coating on a magnesium screw for biodegradable applications, Sci. Rep. 8 (2018) 1–11.
[60] J.F. Navarro-González, C. Mora-Fernández, J. García-Pérez, Reviews: clinical implications of disordered magnesium homeostasis in chronic renal failure and dialysis, in: Seminars in Dialysis, Wiley Online Library, 2009, pp. 37–44.
[61] G. Perumal, B. Ramasamy, S. Dhanasekaran, S. Ramasamy, M. Doble, Bilayer nanostructure coated AZ31 magnesium alloy implants: in vivo reconstruction of critical-sized rabbit femoral segmental bone defect, Nanomed. Nanotechnol. Biol. Med. 29 (2020), 102232.
[62] H. Zhou, B. Liang, H. Jiang, Z. Deng, K. Yu, Magnesium-based biomaterials as emerging agents for bone repair and regeneration: from mechanism to application, J. Magnes. Alloy. 9 (2021) 779–804.